X-ray-induced debromination of nucleic acids at the Br *K* absorption edge and implications for MAD phasing

E. Ennifar,[a] P. Carpentier,[b]
J.-L. Ferrer,[b] P. Walter[a] and
P. Dumas[a]*

[a]UPR 9002 du CNRS, IBMC, 15 Rue
R. Descartes, 67084 Strasbourg CEDEX, France,
and [b]Laboratoire de Cristallographie et
Cristallogenèse des Protéines (LCCP), Institut de
Biologie Structurale J.-P. Ebel CEA–CNRS,
41 Rue Jules Horowitz, 38027 Grenoble
CEDEX 1, France

Correspondence e-mail:
p.dumas@ibmc.u-strasbg.fr

Multi-wavelength anomalous dispersion (MAD) using brominated derivatives is considered a common and convenient technique for solving chemically synthesized nucleic acid structures. Here, it is shown that a relatively moderate X-ray dose (of the order of 5×10^{15} photons mm^{-2}) can induce sufficient debromination to prevent structure determination. The decrease in bromine occupancy with radiation dose can be accounted for by a simple exponential, with an estimated rate constant at the absorption-peak wavelength, 7.4 (0.8) MGy, that is not significantly different from its value at the absorption-edge wavelength, 9.2 (2.6) MGy (the given e.s.d.s assess the relative closeness of the two values, not their absolute accuracy, which is probably worse). Chemically, these results (and others) are consistent with bromine cleavage resulting from direct photodissociation and/or from the action of free electrons, rather than from the action of hydroxyl radicals originating from water dissociation. The free bromine species (Br⁻) diffuse too quickly, even in amorphous ice around 100 K, to allow the determination of a diffusion coefficient. From a practical point of view, it is suggested that a single data collection with a crystal consisting of iodinated instead of brominated derivatives could provide both anomalous scattering and SIR phase information by the progressive cleavage of iodine.

1. Introduction

Nowadays, progress in large-scale chemical synthesis of RNA allows easy substitution of C5-iodo- or C5-bromouridine for uridine at any position in a sequence. Such modified molecules can be of interest for structure determination by providing heavy-atom derivative crystals isomorphous to those obtained with unmodified molecules and/or anomalous scattering phase information. Several RNA structures have been solved by this technique using MIR information (Anderson *et al.*, 1999; Baugh *et al.*, 2000; Correll *et al.*, 1999; Hung *et al.*, 2000; Wild *et al.*, 1999) and MIR(AS) using iodo derivatives (Berglund *et al.*, 2001; Ennifar *et al.*, 1999; Mueller *et al.*, 1999) or bromo derivatives (Ippolito & Steitz, 1998; Scott, 1995; Shah & Brunger, 1999). Modifications of guanines and adenines (C8-halopurine) and of cytosines (C5-halocytosine) are also available for deoxynucleotides, but have rarely been used in RNA crystallography. For the purpose of MAD experiments, bromine is preferred rather than iodine since its *K* edge at 0.9204 Å is easily accessible to tunable-wavelength synchrotron beamlines.

We have tried to use this approach to solve the structure of a dimer of a 23-nucleotide molecule corresponding to the dimerization-initiation site of HIV-1 genomic RNA. However,

we were unable to obtain any interpretable electron-density map. Here, we show that this failure resulted from excessively rapid debromination of bromouridines during irradiation, even though the crystals were kept at 100–110 K. The rate of debromination we observed at the bromine K-edge energy (13.47106 keV) was found to be comparable to the average rate observed with a mixture of bromodeoxyuridine and thymidine irradiated *in vacuo* at 13.43 and 13.51 keV (Furusawa *et al.*, 1996). These observations, as well of those from previous studies (Ravelli & McSweeney, 2000; Burmeister, 2000), are more in favour of radiation-induced damage to frozen crystals resulting from direct photodissociation and in favour of free electrons, rather than of hydroxyl radicals, originating from water dissociation.

2. Methods: sample preparation, crystallization, data collection and dose evaluation

A chemically synthetized 23-nucleotide RNA fragment corresponding to the dimerization initiation site (DIS) of HIV-1(Lai) genomic RNA was purchased from Dharmacon Research Inc. (Lafayette, USA). C5-bromouridine was substituted for uridine at position 3. This bromo-RNA crystallized as a dimer of 23-nucleotide coaxially stacked hairpins (Ennifar, Walter, Ehresmann *et al.*, 2001). Crystals grew as small platelets belonging to the $C222_1$ space group, with one dimer in the asymmetric unit. In this study, the same crystal, approximately $150 \times 100 \times 10$ µm in size and flash-frozen in liquid ethane, was used throughout.

All data were collected at beamline BM30 (ESRF, Grenoble, France) with the crystal maintained around 100 K (no direct measurement of the temperature was performed at the crystal position[1]) in the nitrogen-gas stream delivered by a Cryostream cooler (Oxford Cryosystems, England). A fluorescence spectrum was first acquired in order to accurately locate the bromine K edge (Fig. 1). Data collection on a MAR image plate was started at the absorption peak wavelength (λ_1), immediately followed by collection at the absorption-edge wavelength (λ_2). Another data collection was performed at λ_1 in order to measure accurately the more intense low-resolution reflections. Initial irradiation of the crystal resulted in fluorescence-spectrum measurement (in fact four trials were necessary) and the first 28 images at λ_1, which were discarded. For practical reasons the data collection had to be stopped; the crystal was instantaneously transferred from the nitrogen-gas stream to liquid ethane and kept in liquid nitrogen for two months. It was then reused on the same beamline, but with a MAR CCD, for a third data collection at

[1] There was no indication of any kind of malfunctioning of the cooling device during data collection.

Table 1
Data-collection statistics for MAD experiment on beamline BM30.

Values in parentheses are for the last shell.

Space group	$C222_1$
Resolution (Å)	20–2.6
Unit-cell parameters (Å)	$a = 27.5$, $b = 116.4$, $c = 95.4$

Wavelength	λ_1 peak (0.920184 Å)			λ_2 edge (0.920374 Å)			λ_3 remote (0.917755 Å)
	All data	Peak 1	Peak 2	All data	Edge 1	Edge 2	
Redundancy	3.1	2.7	3.0	3.6	3.0	3.5	4.8
Average $I/\sigma(I)$	23.6 (3.0)	19.6 (8.11)	17.9 (4.7)	22.4 (6.0)	22.8 (7.7)	17.9 (4.1)	30.4 (2.9)
Completeness (%)	98.2 (99.6)	92.4 (96.2)	94.4 (94.5)	99.3 (99.5)	92.1 (96.9)	94.5 (93.7)	99.8 (99.8)
R_{sym} (%)	5.3 (20.3)	4.5 (14.1)	5.1 (24.2)	5.3 (26.1)	3.9 (13.8)	5.4 (31.9)	4.6 (27.3)

a high-energy 'remote' wavelength (λ_3) in order to obtain maximum dispersive differences with λ_2 (Table 1). Data were processed using the *HKL* package (Otwinowski & Minor, 1997).

The photon flux was estimated from measurement of the beam intensity with a photomultiplier protected with a 4 mm thick aluminium screen. The values obtained with collimators of diameter from 0.1 to 0.3 mm agreed well with a resulting flux of about 10^{12} photons $\text{mm}^{-2}\,\text{s}^{-1}$. It should be emphasized that this measurement was not performed immediately before data collection, since the initial goal of this work was certainly not to focus on debromination. Considering that 400 images of $40''$ each were collected from the first X-ray exposure to the end of data collection at λ_2, an irradiation of roughly 1.6×10^{16} photons mm^{-2} is obtained. Burmeister derived for his crystal a dose rate of 7.2×10^6 Gy (J kg^{-1}) for 10^{16} photons mm^{-1}; that is, an overall dose of 3.5×10^7 Gy.
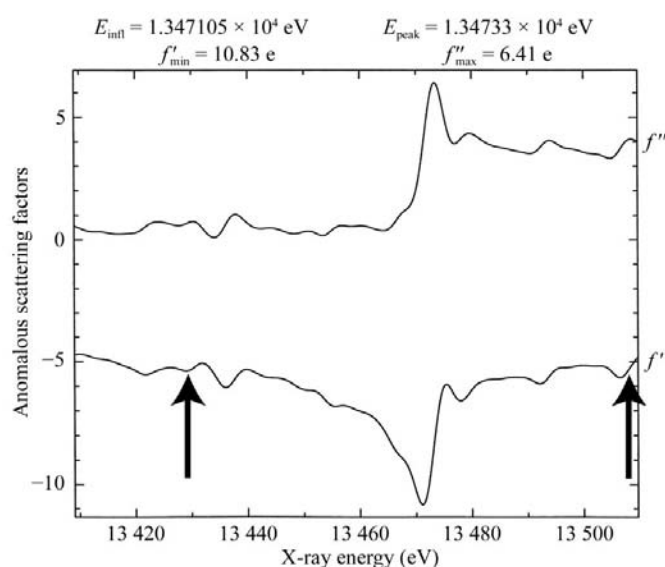

Figure 1
X-ray fluorescence spectrum for the bromo-U3 HIV-1 DIS RNA used in this study (upper curve) and its Kramers–Krönig transform (lower curve) obtained with the program *CHOOCH* (Evans & Pettifer, 2001). The two vertical arrows mark the energies used by Furusawa *et al.* (1996).

Considering that we sought only an order of magnitude, we extrapolated this value to our crystal and obtained an overall dose of 1.2×10^7 Gy at the end of data collection at λ_2. Rough as such an estimate may be, it is sufficient for useful comparisons with other work. All numerical calculations, apart from where stated otherwise, were performed with *Mathematica* 4.01 (Wolfram Research).

3. Proof of radiolysis-induced debromination

The two bromine sites in the asymmetric unit were readily localized with *LOCHVAT* (Dumas, 1994a,b) using anomalous differences at λ_1 ($f'' = 6.4$ e) in the 12–4.0 Å resolution range.
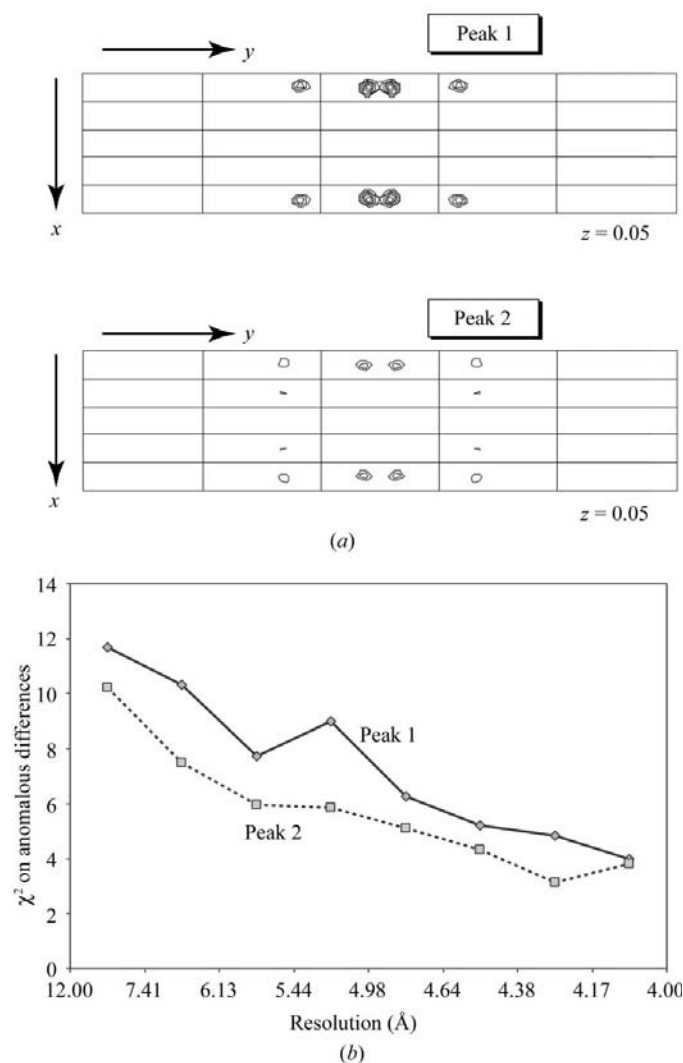

Figure 2
Loss of anomalous signal during data collection at the absorption-peak wavelength. (a) Correlation maps calculated with *LOCHVAT* using anomalous differences of reflections in the 12–4.0 Å resolution range, with reflections from the 75 first (Peak 1) and last (Peak 2) images of the data set. Both maps are represented with the same contour level. The two sites, which turn out to be in the same Z section, appeared clearly with data from Peak 1, but only the less mobile site could be localized with data from Peak 2. (b) Monitoring of the χ^2 of the anomalous signal as a function of resolution for the reflections from Peak 1 and Peak 2 used for the previous correlation maps.

However, only one site could be localized with the dispersive differences between λ_1 and λ_2, and none could be localized with the dispersive differences between λ_2 and λ_3 which should be at a maximum absolute value ($\delta f' = -5$ e). We then tried to solve the structure using *SHARP* (de La Fortelle & Bricogne, 1997) and *SOLVE* (Terwilliger & Berendzen, 1999), but all electron-density maps remained uninterpretable, even after solvent flattening with *SOLOMON* (Abrahams & Leslie, 1996). Eventually, the structure was solved by molecular replacement using independent data from a crystal of non-brominated molecules and a related duplex structure (Ennifar, Walter, Ehresmann et al., 2001) as a model. The structure was refined at 2.6 Å resolution ($R = 20.3\%$, $R_{\text{free}} = 23.5\%$). Further refinement of the brominated structure using data collected at λ_3 revealed a very poor density for both Br atoms in the asymmetric unit, whereas both corresponding uridine bases appeared clearly in the electron-density map. This was indicative of debromination during data collection.

The two data sets collected at λ_1 and λ_2 were reprocessed by dividing each of them into two halves, named Peak 1, Peak 2 for λ_1, and Edge 1, Edge 2 for λ_2, while maintaining sufficient completeness and redundancy. This was not possible for the data set at λ_3, which was thus kept as a single data set (Table 1). We then calculated correlation maps with *LOCHVAT* in the 12–4.0 Å resolution range, using anomalous differences for Peak 1 and Peak 2 (Fig. 2a). A very significant loss of the signal-to-noise ratio is observed for Peak 2 *versus* Peak 1 data since the 'minor' bromine site (in fact corresponding to the uridine with the highest temperature factor) has disappeared, whereas it is fully visible for Peak 1 data. This shows that the decrease in bromine discernability is already apparent within the first data set and is not the result of problems arising from comparisons between different data sets. This was also assessed by monitoring the χ^2 value defined as the average of $(F^+ - F^-)^2/[\sigma^2(F^+) + \sigma^2(F^-)]$ in each resolution shell (Fig. 2b). As expected, its value drops significantly from Peak 1 to Peak 2.

Debromination is clearly apparent in difference Fourier maps with coefficients $(F_{\text{obs}} - F_{\text{calc}})$, the F_{calc} values being obtained after refinement with *CNS* (Brünger et al., 1998) of the bromine-free model against the five available data sets (Fig. 3a). R_{free}-factor variations further strengthen our interpretation by showing that the lowering of peak height at the bromine positions in the successive difference maps is not a consequence of a loss of data quality with increasing exposure. Indeed, the highest R_{free} value was obtained with the first data set (shortest exposure) and the lowest one with the last data set (longest exposure) (Fig. 3b). This is consistent with the continuous decrease of bromine occupancy from the beginning to the end of data collection and with the absence of bromine in the model used for refinement. Noticeably, the R_{free} factors obtained either with data collected at λ_3 (longest exposure) or with data collected in a shorter time with the bromine-free structure are comparable (22.4 and 23.5%, respectively). Therefore, although debromination was almost complete at this stage of data collection, the overall quality of the data was not considerably affected after the longest

exposure, apart for a significant increase from 34.7 to 45.8 Å^2 in the overall temperature factor. This confirms that debromination is a rather fast process in comparison to other radiation-induced damage in the solid state around 100 K.

We refined the bromine occupancies with the different data sets. The temperature factor of each Br atom was held fixed to the value of the temperature factor of the C5 atom to which it is covalently bound (20 and 42 Å^2). Refinement was started with Peak 1 data with a model having two fully occupied

Figure 3
Occupancy decrease of bromine sites. (a) σ_A-weighted ($F_{obs} - F_{calc}$) difference maps calculated in the 10–2.6 Å resolution range around uridine 3 of one strand (corresponding to the less mobile Br site), with reflections from Peak 1, Peak 2, Edge 1, Edge 2 and remote-wavelength data sets. The map is contoured at the 5.3σ level. The given doses correspond to the cumulative dose used in Fig. 3(b) for each data set (i.e. the doses at mid-time of each data collection). The last value for the remote wavelength (13.4 MGy) is an uncertain extrapolation that was not used for the quantification described in the text. (b) Variation of the refined occupancy for the two bromine sites and of the R_{free} factor versus the cumulative dose (see text). The smoother variation of Occ1 in comparison of Occ2 is an indicator of the better quality of this set of occupancies owing to the lower thermal agitation of the corresponding Br atom.

bromine sites. The resulting model (with the refined occupancies of the bromine sites) was used, after heating to 600 K, as the starting model for refinement with Peak 2 data and the same procedure was repeated analogously with the other three data sets. The resultant occupancies are shown in Table 2 and their quality is reasonably assessed by the closeness of the values for both sites at each step (Occ1 and Occ2 in Table 2 and Fig. 3b).
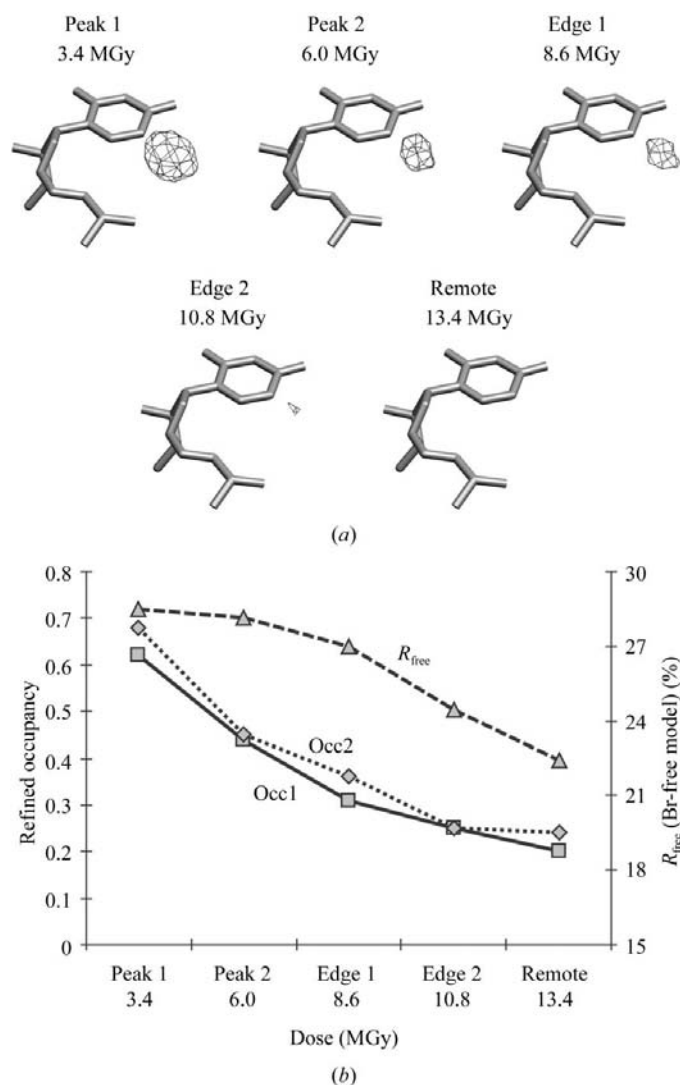
4. Quantification of the radiolysis dose-dependence

The set of varying occupancies for the site with the lower temperature factor (Occ1 in Table 2), a priori the most accurately determined, was used to derive parameters for the dose-dependence of radiolysis. It should be noticed first that any occupancy value previously obtained corresponds to a dose-averaged value during data acquisition, particularly because, as mentioned above, bromine radiolysis is rather fast. This implies that a prior hypothesis is necessary to deconvolute the experimental data. It is well known in radiation chemistry that radiolysis can result directly from radiation-induced ionization, but that the majority of radiolytic events in aqueous solution originate from several unstable species resulting from dissociation of water (and in turn producing other unstable species): the uncharged radicals OH˙, H˙ or molecule H_2O_2 and the charged species H_3O^+, ˙H_2O^+, OH^- and e_{aq}^-, the latter being the hydrated electron (for short reviews and additional references, see Ravelli & McSweeney, 2000; Weik et al., 2000; Burmeister, 2000). Under such conditions, a linear dependence of the effect (the amount of appeared or disappeared molecules) on the radiation dose absorbed by the sample is often observed, whereas a purely photochemical effect (essentially a first-order mechanism) would lead to an exponential dependence. Such a linear dependence of debromination on the absorbed dose is well illustrated by a study on γ-ray damage to a millimolar aqueous solution of 5-BrUMP (Greenstock & Whitehouse, 1992). Interestingly, it showed 75% debromination after a dose of $\sim 1.5 \times 10^3$ Gy, i.e. four orders of magnitude less than the dose necessary to produce the same effect under the conditions of our study. Since diffusion is not abolished around 100 K (see below), it may be asked whether radiolysis in the crystalline state at such a temperature proceeds through a chemical process involving essentially the same radicals but at a much slower rate, or by a different mechanism. Interestingly, work by Ravelli & McSweeney (2000) and Burmeister (2000) has shown no significant correlation between the numerous damaged chemical groups and their accessibility to solvent. Burmeister, for example, reported that the most labile methionine methylthio group is deeply buried inside the protein hydrophobic core. These examples are indicative of a minor role of active radicals such as OH˙ (although a marginal correlation with accessibility was observed by Weik et al., 2000). Together, these considerations favour a direct photochemical effect for bromine radiolysis in a frozen crystal, particularly at the Br-absorption peak wavelength, where the photoabsorption cross-section is at a maximum. Secondary electrons produced

by ionization should also have a significant role, since it is known that iodo- or bromobenzene, which are comparable to bromouridine, are efficiently dissociated by thermalized e_{aq}^- into I^- or Br^-, respectively, and $\cdot C_6H_5$ (Anbar & Hart, 1964). Whether e_{aq}^-, which requires a dynamic favourable orientation of several water molecules, is significantly present at 100 K is questionable, but free migrating electrons (within a macromolecule; Ravelli & McSweeney, 2000) should be present, possibly at a much lower concentration than their hydrated form, which is able to accumulate.

The previous considerations, as well as the observations by Burmeister (2000) on the dependence of the occupancies of all labile groups on the dose d absorbed by the crystal, led us to consider that the occupancy of bromine varied as

$$q(d) = \exp(-d/D), \qquad (1)$$

D being a constant depending *a priori* on the wavelength. Therefore, the average occupancy value between d_1 and d_2 is given by[2]

$$\overline{q}_{d_{1\to 2}} = \frac{D[\exp(-d_1/D) - \exp(-d_2/D)]}{d_2 - d_1}. \qquad (2)$$

To take into account the different values of D that might be necessary for different wavelengths, (2) was used to fit Peak 1 and Peak 2 occupancies, and the following modified form (2′) to fit Edge 1 and Edge 2 occupancies:

$$\overline{q}_{d_{2\to 3}} = \exp(-d_1/D_1)\frac{D_2[\exp(-d_2/D_2) - \exp(d_3/D_2)]}{d_3 - d_2}. \qquad (2')$$

In (2′), D_1 and D_2 correspond to values of D for λ_1 and λ_2, respectively, d_1 to the cumulative dose received during prior irradiation at λ_1, and d_2 and d_3 to the additional cumulative doses received during irradiation at λ_2 (thus, d_2 is zero for Edge 1). The dose received for each image during a particular data collection was considered to be proportional to the average pixel value in this image. Since the crystal was irradiated by an unknown dose before the true data collection at λ_1, all cumulative doses [d_1 and d_2 in (2) and d_1 in (2′)] were increased by a refinable amount d_0.

It was not attempted to derive the value of D for λ_3 because the difficulty of comparing the irradiation dose at this wavelength (using a MAR CCD) with the doses at λ_1 and λ_2 (using a MAR image plate) and the inherent imprecision in determining correctly a weak occupancy (∼0.2) increased the level of errors too much. Clearly, an independent measure would be necessary to derive this value.

It was attempted to derive a value for the diffusion coefficient of the free bromine species (most likely Br^-) in amorphous ice at 100–110 K. This failed because the diffusion was much too rapid compared with both the radiolysis and data-collection timescales to permit such a determination. This is

[2] Calculation shows that if one considers a moving window of constant width $\delta = (d_2 - d_1)/D$ between doses d_1 and d_2, then the average occupancy value given by (2) corresponds to an 'instantaneous' occupancy value given by (1) at a point displaced from the average dose $(d_1 + d_2)/2$ by a constant shift $-D\log[\sinh(\delta/2)/(\delta/2)]$. This yields a very minor correction which was taken into account.

Table 2
Quantification of bromine radiolysis dose-dependence.

Data sets	Zero†	Peak 1	Peak 2	Edge 1	Edge 2	Peak 3‡	Remote
Dose§ (MGy)	$d_0 = 2.2$	2.4	2.8	2.2	2.2	0.14	—
Occ1 (exp.)¶	—	0.62	0.44	0.31	0.25	—	0.20
Occ2 (exp.)¶	—	0.68	0.45	0.36	0.25	—	0.24
Occ1 (theor.)††	—	0.620	0.436	0.320	0.253	—	—

† Prior irradiation for absorption spectrum measurement and 28 unused images (the value of d_0 was obtained from from fitting Occ1 to the exponential model). ‡ Peak 3: measurement of intense low-resolution data at λ_1. § Absorbed X-ray dose for each data set (1 MGy = 10^6 Gy = 10^6 J kg^{-1}). ¶ Bromine occupancies obtained by model refinement (see text). †† Bromine occupancy derived from fitting Occ1 values to the exponential model.

consistent with measurements of the movement of HCl in ice at 190 K, which have shown diffusion over distances as large as 10^4 Å within only 2 min (Livingston *et al.*, 2000).

5. Results and discussion

With this exponential model, we obtained the radiolysis rate at the peak wavelength [$D_1 = 7.4$ (0.8) MGy] and at the edge wavelength [$D_2 = 9.2$ (2.6) MGy]. The given values, corresponding to averages, and their standard deviations were obtained from repeated calculations with 1000 sets of synthetic occupancy data differing from those in Table 2 by random normal errors with an e.s.d. of 0.02 (this value was considered reasonable from the observed differences between Occ1 and Occ2; see Table 2 and Fig. 3*b*). The scattergram of the results (not shown) reveals, as expected, an inverse correlation of D_1 and D_2 fitted approximately by $(D_2 - 9.2) = -2(D_1 - 7.4)$. On the basis of our data, the average values and e.s.d.s of their difference [$\langle(D_2 - D_1)\rangle = 1.8 \pm 3.2$ MGy] and of their ratio [$\langle(D_2/D_1)\rangle = 1.3$ (0.5)] indicate that D_1 and D_2 are not significantly different from their weighted average $D = 8.0$ (0.8) MGy. However, this is not a firm conclusion.

It should be recalled that these absolute values depend on the rather crude estimate of the overall dose received by the crystal (§2). Therefore, the given e.s.d.s for D_1 and D_2 assess their relative closeness, not their absolute accuracy, which is probably worse. The fact that there are three refinable parameters (d_0, D_1 and D_2) for only four occupancy values to be fitted implies that the result may be viewed as poorly significant even though the fit is excellent (Table 2). Also, trying to fit the data with a simple linear dependency yielded almost as good a fit. However, the obtained value for the predose d_0 seemed unreasonably high (1.9 times the dose used for Peak 1), whereas its value for the exponential model was in the expected range (0.9 times the dose used for Peak 1). In addition, the results by Burmeister, which involve much slower radiolysis events and therefore yield less dose-averaged occupancy values, support our hypothesis.

It is interesting to compare these results with those obtained *in vacuo* at ambient temperature with bromodeoxyuridine (BrdU) alone, or mixed with deoxythymidine (dT), after irradiation with monoenergetic X-rays on both sides of the same absorption edge (13.43 and 13.51 keV; arrows in Fig. 1; Furusawa *et al.*, 1996). This study led to significant differences

for these more distant wavelengths since radiolysis was 2.5 times more efficient at 13.51 keV than at 13.43 keV. The authors also concluded that there was a linear relationship between the yield of radiolytic products and the X-ray dose. This seems contradictory to our hypothesis since their study was conducted *in vacuo*, which implies (even more certainly than in our frozen crystals) that neither hydroxyl radicals nor hydrated electrons, but only photons and free electrons, could have been significantly involved in radiolysis. However, we think the contradiction is only apparent, as Furusawa and coworkers reported on X-ray doses ($<10^4$ Gy) yielding in the dry state less than 3 mmol of products per mole of BrdU. Therefore, the observed linear relationship merely corresponds to a tangent at the origin. Considering an average value of their results for the two wavelengths (their Figs. 4 and 5), we obtained an estimate for D of either 20 MGy for BrdU alone or 4 MGy for BrdU plus dT. Keeping in mind the approximations that we have made and the important differences in the experimental systems, their values fit well with the value of 8.0 (0.8) MGy from our data. The most significant and unambiguous difference with our study is that Furusawa and coworkers observed the production of Br^- and of uridine base. We did not observe in the present crystal study any significant sign of such base cleavage accompanying bromine radiolysis. It cannot be excluded that if this occurred, the base was held fixed by the low temperature and favourable stacking interaction.

Finally, it would be interesting to test directly our belief that hydroxyl radicals are not the main cause of radiolysis. Since many compounds are known as efficient hydroxyl radical scavengers (Aruoma, 1994) and that among them are found efficient cryoprotectants (glucose and glycerol), it might be possible to test whether or not there is a negative correlation between their concentration and radiolytic damages.

6. Practical conclusions for MAD phasing

Our results provide a reasonable estimate for a maximum dose to be used on a given crystal to avoid pronounced bromine radiolysis. This is evidently of practical interest if the beam intensity is known. However, it is now clear that the beam intensity and not only the overall dose is an important factor in radiolytic damage (Schrøder Leiros *et al.*, 2001). It is quite possible that overly intense X-ray beams simply result in significant heating of the crystals (Kuzay *et al.*, 2001). As already stated by Burmeister (2000), larger crystals, if available, should be preferred for such a MAD experiment since they would require a weaker dose (*i.e.* less photons absorbed per unit of mass of scattering material) for a given average value $I/\sigma(I)$. It should also be recalled that with crystals of sufficient size, a procedure as simple as a slight displacement in the beam might well rescue a data collection that would otherwise be useless. Towards this goal, a simple mechanical device coupling a crystal translation to its rotation about the spindle axis might be useful. When the available crystals are too small and although common practice does not favour it for MAD data collection, one should also consider as a valuable

alternative the use of more than one crystal. Evidently, the best compromise for the number of crystals heavily depends on its Laue symmetry. Concerning the choice of a third 'remote wavelength', Fig. 1 shows that either sides of the K edge are equivalent for maximizing the dispersive difference with the edge wavelength. However, if extrapolating the results by Furusawa and coworkers ($D_{13.43 \text{ keV}}/D_{13.51 \text{ keV}} = 2.5$) is valid, the low-energy side is a much better choice to minimize radiolytic damage. This needs to be verified. It has also been reported for a 26-nucleotide RNA that a two-wavelength MAD experiment can produce better results than a three-wavelength MAD experiment for structure determination (Hung *et al.*, 2000).

It is also tempting to suggest to turn the adverse effect described in this paper into a beneficial one. Indeed, by using an iodo derivative instead of a bromo derivative, one could measure data with a valuable anomalous signal ($f'' > 5$ e for $\lambda > 1.3$ Å) and after sufficient irradiation of the crystal one could measure data for the 'native' form of the crystal after deiodination. The significantly higher Z value for iodine (53 compared with 35 for bromine) should allow solution of the structure by the SIRAS method, possibly supplemented by solvent flattening which has often been shown to be extremely efficient. Interestingly, a single data collection, provoking a continuous drift from fully occupied to (nearly) vacant iodine sites, could be sufficient provided that the phasing software could handle iodine occupancies continuously varying in time. Our results show that a simple exponential dependence, with only one parameter to be refined, should accurately describe the iodine-occupancy variation and in turn allow reliable temperature-factor refinement. Evidently, this requires abandoning the usual merging of data by averaging of equivalent reflections and keeping each intensity separate along with the overall dose received by the crystal when it was measured.

Finally, it should also be kept in mind that a valuable alternative to halo derivatives for structure determination of relatively short RNA fragments is exchanging the magnesium commonly bound to RNA for zinc (Ennifar, Walter & Dumas, 2001). Zinc has some significant advantages over bromine for MAD experiments: its K edge presents a broader white line at the absorption peak (which reduces the probability of using an incorrect wavelength owing to limitations in energy resolution on beamlines) and the maximum f'' value is slightly higher than that of bromine.

References

Abrahams, J. P. & Leslie, A. G. W. (1996). *Acta Cryst.* D**52**, 30–42.
Anbar, M. & Hart, E. J. (1964). *J. Am. Chem. Soc.* **86**, 5633–5637.
Anderson, A. C., O'Neil, R. H., Filman, D. J. & Frederick, C. A. (1999). *Biochemistry*, **38**, 12577–12585.
Aruoma, O. I. (1994). *Methods Enzymol.* **233**, 57–66.
Baugh, C., Grate, D. & Wilson, C. (2000). *J. Mol. Biol.* **301**, 117–128.
Berglund, J. A., Rosbash, M. & Schultz, S. C. (2001). *RNA*, **7**, 682–691.

Brünger, A. T., Adams, P. D., Clore, G. M., Delano, W. L., Gros, P., Grosse-Kunstleve, R. W., Jiang, J. S., Kuszewski, J., Nilges, M., Pannu, N. S., Read, R. J., Rice, L. M., Simonson, T. & Warren, G. L. (1998). *Acta Cryst.* D**54**, 905–921.

Burmeister, W. P. (2000). *Acta Cryst.* D**56**, 328–341.

Correll, C. C., Wool, I. G. & Munishkin, A. (1999). *J. Mol. Biol.* **292**, 275–287.

Dumas, P. (1994*a*). *Acta Cryst.* A**50**, 526–537.

Dumas, P. (1994*b*). *Acta Cryst.* A**50**, 537–546.

Ennifar, E., Walter, P. & Dumas, P. (2001). *Acta Cryst.* D**57**, 330–332.

Ennifar, E., Walter, P., Ehresmann, B., Ehresmann, C. & Dumas, P. (2001). *Nature Struct. Biol.* **8**, 1064–1068.

Ennifar, E., Yusupov, M., Walter, P., Marquet, R., Ehresmann, B., Ehresmann, C. & Dumas, P. (1999). *Structure*, **7**, 1439–1449.

Evans, G., & Pettifer, R. F. (2001). *J. Appl. Cryst.* **34**, 82–86.

Furusawa, Y., Maezawa, H., Takakura, K., Kobayashi, K. & Hieda, K. (1996). *Acta Oncol.* **35**, 877–882.

Greenstock, C. L. & Whitehouse, R. P. (1992). *Radiat. Environ. Biophys.* **31**, 1–9.

Hung, L. W., Holbrook, E. L. & Holbrook, S. R. (2000). *Proc. Natl Acad. Sci. USA*, **97**, 5107–5112.

Ippolito, J. A. & Steitz, T. A. (1998). *Proc. Natl Acad. Sci. USA*, **95**, 9819–9824.

Kuzay, T. M., Kazmierczak, M. & Hsieh, B. J. (2001). *Acta Cryst.* D**57**, 69–81.

La Fortelle, E. de & Bricogne, G. (1997). *Methods Enzymol.* **276**, 472–494.

Livingston, F. E., Smith, J. A. & George, S. M. (2000). *Anal. Chem.* **72**, 5590–5599.

Mueller, U., Muller, Y. A., Herbst-Irmer, R., Sprinzl, M. & Heinemann, U. (1999). *Acta Cryst.* D**55**, 1405–1413.

Otwinowski, Z. & Minor, W. (1997). *Methods Enzymol.* **276**, 307–326.

Ravelli, R. B. & McSweeney, S. M. (2000). *Structure Fold. Des.* **8**, 315–328.

Schrøder Leiros, H.-K., McSweeney, S. M. & Smalas, A. O. (2001). *Acta Cryst.* D**57**, 488–497.

Scott, W. G. (1995). *Cell*, **81**, 991–1002.

Shah, S. A. & Brunger, A. T. (1999). *J. Mol. Biol.* **285**, 1577–1588.

Terwilliger, T. C. & Berendzen, J. (1999). *Acta Cryst.* D**55**, 849–861.

Weik, M., Ravelli, R. B., Kryger, G., McSweeney, S., Raves, M. L., Harel, M., Gros, P., Silman, I., Kroon, J. & Sussman, J. L. (2000). *Proc. Natl Acad. Sci. USA*, **97**, 623–628.

Wild, K., Weichenrieder, O., Leonard, G. A. & Cusack, S. (1999). *Structure Fold. Des.* **7**, 1345–1352.